



Modeling of discharge capacity of H-weir using experiments, bio-inspired optimization and data preprocess based on SVM

V. Kartal¹ · M. Emin Emiroglu² · O. M. Katipoglu³

Received: 9 December 2023 / Revised: 19 January 2024 / Accepted: 30 January 2024 / Published online: 28 February 2024

© The Author(s) under exclusive licence to Iranian Society of Environmentalists (IRSEN) and Science and Research Branch, Islamic Azad University 2024

Abstract

H-weir is a combination of a rectangular gate and weir. Side weirs are applied to discharge flow and regulate the flow height. The present study presents the modeling of the H-side weirs using experiments and optimization based on SVM in a straight channel under free and subcritical flow conditions. The geometrical and flow parameters affecting the discharge capacity were determined based on dimensional analysis. The findings show that the weir flow is not in contact with the flow below the gate with increased vertical distance between the weir crest and gate top (d) and the upstream Froude number (F_1). It was found that the discharge capacity of the H-side weir is 1.3–4.0 times higher than conventional side weirs and 1.6–9.0 times higher than side gates under the same conditions. Moreover, a discharge equation is derived from a/y_1 , h/b , b/B , F_1 and d/a with an absolute percentage error of about 5.84%. The most successful model for predicting the discharge of the H-side weir was VMD-LSSVM. In addition, it was concluded that the established LSSVM, PSO-LSSVM and PSO-VMD-LSSVM models produced very satisfactory predictions.

Keywords Open channel flow · H-weir · Discharge capacity · Optimization · Data preprocessing

List of symbols

a	Opening of side sluice gate (m)	g_{best}	Best neighbor solution position
B	Width of main channel (m)	h	Piezometric head over the weir (m)
b	Length of side structure (m)	p	Crest height (m)
C	Regularization constant	p_i	Best individual solution position
c_1, c_2	Acceleration constants	Q	Discharge (m^3/s)
C_d	Discharge coefficient (–)	q	Unit discharge ($\text{m}^3/\text{s m}$)
d	Distance between the top of the sluice gate and the weir crest (m)	q_t	Dimensionless unit discharge ($\text{m}^3/\text{s m}$)
e_i	Training data error	Re	Reynolds number (–)
E	Specific energy (m)	S_0	Slope of the main channel (–)
F	Froude number (–)	S_f	Slope of friction (–)
φ	Deflection angle of the streamlines ($^\circ$)	v_i	Velocity
g	Acceleration due to gravity (m/s^2)	V	Flow velocity (m/s)
		We	Weber number (–)
		x	Distance along the side structure (m)
		x_i	Indicate position
		ω	Inertia weight
		y	Flow depth (m)
		α	Kinetic energy coefficient (–)
		ϕ	Varied flow function
		φ	Deflection angle of the streamlines ($^\circ$)
		η	Outflow efficiency (–)
		η_1, η_2	Random vectors
		μ	Dynamic viscosity ($\text{kg}/\text{m s}$)
		ρ	Mass density of water (kg/m^3)
		σ	Surface tension (kg/s^2)

Editorial responsibility: Shahid Hussain.

✉ V. Kartal
vkartal@firat.edu.tr

¹ Department of Civil Engineering, Siirt University, 56000 Siirt, Turkey

² Department of Civil Engineering, Firat University, 23119 Elazig, Turkey

³ Department of Civil Engineering, Erzincan Binali Yildirim University, 24000 Erzincan, Turkey



Subscripts

c	Combined side weir–gate
e	Estimated
g	Side sluice gate
m	Measured
w	Side weir
1	Upstream section of H-side weir
2	Downstream section of H-side weir

Introduction

Structures that allow water to be used for various purposes of control are called hydraulic structures. Engineering applications such as hydroelectric and wave energy generation, environmental regulation and recreation areas, irrigation water supply, drinking and utility water supply, coastal and harbor structures, urban drainage, wastewater management and flood control are among the main areas of use of water engineering structures (Novák and Cabelka 1981). Scale effect in hydraulic structures is vital for analyzing these structures (El Baradei et al. 2022; Yamini et al. 2021). Excellent and reliable results are obtained in the laboratory models with the appropriate scale (Al-Bedyry et al. 2023; Qasim et al. 2022).

Side weirs are vital hydraulic applications specifically designed to regulate the flow or water level of the stream. Side weirs are frequently utilized to remove excess water from any channel or to provide the required flow rate. Side weirs are applied as lateral intake spillways in irrigation systems, land drainage, surface water removal, urban combined sewerage systems, removal of water considered clean above a certain depth, hydroelectric dams and flood protection structures. Placing the spillway on the dam body is impossible in dams constructed in narrow valleys. The spillway crest at normal water level can be designed as a lateral intake spillway parallel to the dam reservoir to solve this problem. In the late 90 s, Ahmed (1985) pioneered the study of combined weirs and gates in open channels. Since then, many studies have been conducted on combined weir–gate models for frontal flow (Alhamid et al. 1997; Alhamid 1999; Altan-Sakarya and Kökpınar 2013; Askeroğlu 2006; Negm et al. 2002; Parsaie et al. 2017, 2018, 2018; Samani and Mazaheri 2009; Salehi and Azimi 2019; Nouri and Hemmati 2020; Altan-Sakarya et al. 2020; Azamathulla et al. 2019).

Combined weir–gate structures can be built to regulate the water level, control the flow, take water and measure the flow rate in rivers and open channels. Combined weir–gate structures can be constructed in different geometric shapes. Combined weir–gate structures are also used to obtain hydrological data, the control section of water supply channels and diversion structures. Many studies in the literature

on weirs and gates show that they operate separately from each other. Weirs and gates are applied in many hydraulic engineering applications in open channel flows, especially for frontal flows. They have advantages and disadvantages. Namely, the accumulation of sediment from the stream or reservoir from which the water is taken over time behind the weir and the accumulation of floating materials behind the gates cause measurement errors and operation and maintenance difficulties and reduce the operating life of these structures. It aims to reduce the problems that have occurred or will occur by ensuring the passage of the material that will accumulate behind the weir and gate. In this way, both the safety and lifetime of the structure will increase, and at the same time, eliminating the problems caused by accumulation will increase the preferability of these structures (Altan-Sakarya and Kökpınar 2013; Askeroğlu 2006; Azamathulla et al. 2019). For this purpose, many weir–gate structures with different geometries have been studied in the literature. However, in practice, combined rectangular weir–gate structures are more common. There are many studies on combined weir–gate in the literature. However, these studies are related to structures with frontal flows. It is not easy to make precise statements about the performance of the sediment passage through the gate and the passage of floating materials through the weir in lateral flows. Researchers have already noted these advantages of combined weir–gate structures for frontal flows. Detailed experimental studies are needed for sediment passage in lateral flows.

For this reason, it is also clear that there will be differences in sediment passage in lateral flows. Weirs and gates have been used independently of each other in open channel flows for a long time in hydraulic engineering. Combined weir–gate structures in frontal flow are frequently mentioned in the literature for the passage of accumulated materials downstream under gates and the passage of floating materials downstream over the weir (Altan-Sakarya and Kökpınar 2013; Askeroğlu 2006; Negm et al. 2002; Parsaie et al. 2017, 2018).

Alhamid (1999) studied the combined flow using triangular weir and rectangular gate structures. The author stated that the combined flow is complex because of the mixing of over-weir and under-gate flows and the number of parameters affecting the flow characteristics. Askeroğlu (2006) investigated the combined flow over trapezoidal weirs and under rectangular gates. The combined flow was evaluated by examining the dimensionless unit discharge value obtained from the dimensional analysis. It was determined that the variation of the combined flow with the dimensionless parameters (bla , Reynolds and Weber numbers) in this equation is negligible. As a result, the combined flow was analyzed by considering the hydraulic parameters (y_1/a and h/b) and the geometric parameters (d/a and b/B) (Fig. 1). The researcher proposed equations to estimate the dimensionless



unit discharge using multiple regression. The author proposed the following equation to estimate the discharge of combined flow.

$$\frac{Q_c/b}{\sqrt{2ga^{1.5}}} = -1.9808 + 1.5240\left(\frac{y_1}{a}\right) + 0.0949\left(\frac{h}{b}\right) - 1.3918\left(\frac{d}{a}\right) + 0.0840\left(\frac{B}{b}\right) \quad (1)$$

Negm et al. (2002) investigated experimentally combined flow characteristics using sharp-crested rectangular weirs and gates for free-flow conditions. The researchers stated that the viscosity effect could be neglected for Reynolds number $Re > 200,000$, and surface tension can be ignored for Weber number $We > 40$. Negm et al. (2002) discussed hydraulic and geometric effects on the simultaneous discharge, i.e., the combined flow rate. Negm et al. (2002) proposed the following equation to estimate combined discharge.

$$\frac{Q_c/b}{\sqrt{2ga^{1.5}}} = -0.3863 + 0.8764\left(\frac{y_1}{a}\right) - 0.1494\left(\frac{h}{b}\right) - 0.7341\left(\frac{d}{a}\right) \quad (2)$$

Altan-Sakarya and Kökpinar (2013) experimentally investigated the simultaneous flow over the weir and under the gate in frontal flows under free-flow conditions. They named this structure, a combination of a rectangular weir with a sharp crest and a rectangular gate, an H-weir and considered it a flow measurement structure. They defined H-weirs by the weir length and gate opening, gate opening and the vertical distance between the bottom of the weir, i.e., the crest and the top of the gate opening. This experimental study measured water depth upstream and flow rates using different H-weir models.

Parsaiea and Haghiabi (2021) predicted the discharge coefficient of the combined weir–gate via soft computing techniques. The authors analyzed the combined weir–gate by considering the contraction ratio (b/B), the ratio of the vertical distance from the top of the gate opening to the crest (d/a), the ratio of the weir length to the opening of the weir–gate (b/a) and the ratio of the upstream flow depth to the gate opening (y_1/a).

Altan-Sakarya et al. (2020) numerically investigated combined weir–gate models. The researchers emphasized that accumulating weir and gate formulations cannot calculate the combined discharge. Furthermore, they stated that the discharge coefficient values of the weirs and gates are different and larger than the experimental values. Soft computing methods have been widely used in estimating discharge capacity due to the complex relationships of discharge capacity between various geometric and hydraulic conditions. Many researchers attempted to use soft computing techniques to solve the drawbacks of extensive calculations and inappropriate use of empirical (Ayaz et al. 2023;

Bonakdari and Zaji 2018; Elshaarawy and Hamed 2024; Ismael et al. 2021; Li et al. 2023; Norouzi et al. 2019; Parsaie 2016; Parsaie et al. 2018, 2023; Parsaie and Haghiabi 2016; Razmi et al. 2022; Roushangar et al. 2018; Salmasi et al. 2021; Seyedian et al. 2023; Simsek et al. 2023; Zaji et al. 2016). Tao et al. (2022) used the learning model to predict the discharge coefficient patterns of the gate flow under free-flow and submerged flow conditions. Ismael et al. (2021) used neural network technology to predict the discharge coefficient of inclined cylindrical weirs with different diameters. Chen et al. (2022) proposed to predict the discharge coefficient of aerodynamic weirs, and the results showed that hybrid deep data-driven algorithms provide more accurate results than classical ones. Simsek et al. (2023) used an artificial neural network (ANN) to estimate the discharge coefficient of a trapezoidal broad-crested weir. They found that the ANN method was more successful than other methods in determining the flow coefficients. Balouchi and Rakhshandehroo (2018) applied soft computing models to assess the discharge coefficient for combined weir–gate and found that the multilayer perceptron outperformed.

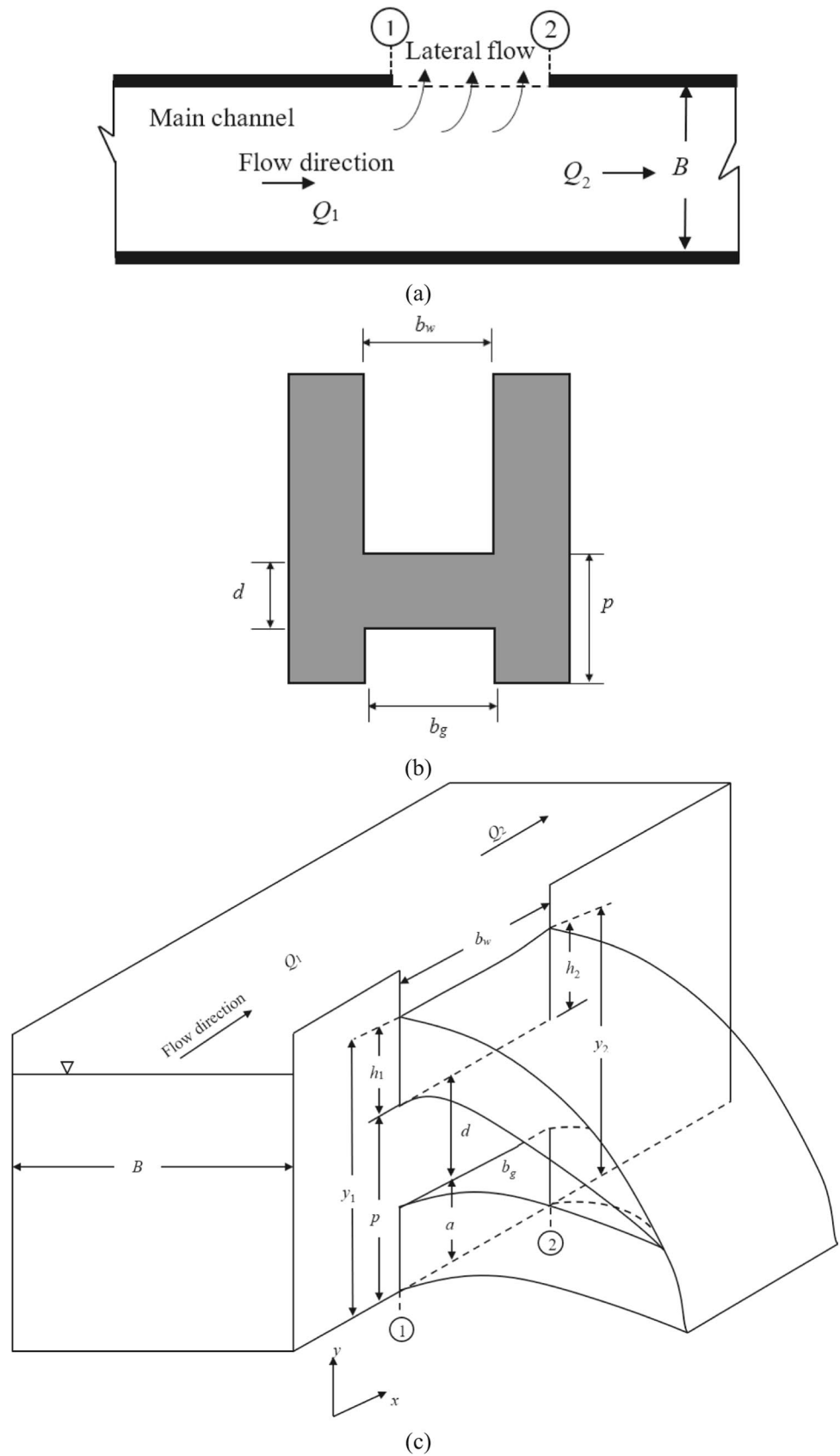
When the literature is examined, we have found that limited studies are related to using combined weir and gate structure as a water intake structure in lateral flows in open channels (Ghodsian et al. 2020; Kartal 2022; Kartal and Emiroglu 2022). Ghodsian et al. (2020) studied the effect of the upstream Froude number (F_1), the ratio of the vertical distance between the gate top and the crest to the gate opening (d/a), the ratio of the upstream flow depth to the gate opening (y_1/a) and the angle of curvature (α) on the discharge capacity for subcritical flow regime. The researchers found that the discharge coefficient of the combined side weir–gate is a decreasing function of F_1 and d/a . It was also found that as y_1/a increases, the discharge coefficient increases, i.e., y_1/a is also an increasing function. The researchers emphasized that the results obtained from this study are limited to $0.12 < F_1 < 0.63$, $53 \leq \alpha \leq 115^\circ$, $0.75 \leq d/a \leq 2.0$, $1.9 \leq y_1/a \leq 6.9$ and $b/B = 0.616$. While analyzing the combined flow, the researchers took the combined side weir–gate discharge as $Q_c = Q_g + Q_w$.

$$Q_c = C_{dg}ab_g\sqrt{2gy_1} + \frac{2}{3}C_{dw}b_w\sqrt{2g}(y_1 - p)^{\frac{3}{2}} \quad (3)$$

$$\text{Discharge coefficient of combined side weir - gate: } C_d = \frac{Q_c}{Q_w + Q_g} \quad (4)$$

It is aimed to increase the discharge capacity by using such structures in lateral flows. However, to our knowledge, there are limited studies on using combined side weir–gate in lateral flows in straight channels (Ghodsian et al. 2020; Kartal 2022; Kartal and Emiroglu 2022). Therefore, this study analyzes H-side weir flow and determines its advantages

Fig. 1 Flow characteristics of H-side weir: **a** plan, **b** cross-sectional view and **c** side view



over classical side weir and gate structures based on dimensional analysis.

The present study experimentally investigated H-side weir flow for different Froude numbers and different flow depths in lateral flows under free-flow conditions and sub-critical regimes in a straight channel. Moreover, the study aims to determine the discharge capacity, reveal the flow characteristics, determine the hydraulic performance and increase the discharge capacity for the same length and estimate the H-side weir discharge capacity by combining various artificial intelligence, bio-inspired optimization and data decomposition techniques using geometrical parameters (d/a) and flow parameters. Furthermore, least-squares support-vector machines (LSSVM), particle swarm optimization (PSO) and variable mode decomposition (VMD) algorithms are combined. Moreover, it aims to contribute to hydraulic engineering by using a new hydraulic structure in addition to classical weirs and gates in lateral flows. The effect of flow and geometric properties on the discharge capacity was analyzed with a wide range of experiments on the combined models of a rectangular weir and a rectangular gate (H-weir). The results will contribute to the limited literature on the subject, pioneer future studies and fill the gaps in the related field.

Materials and methods

Weirs and gates have been used in hydraulic engineering for a long time independently of each other in open channel flows. H-weir is a combination of a gate and a weir. Figure 1 shows the flow characteristics of the H-side weir.

Experiments

The experiments were conducted in the Hydraulic Laboratory at Firat University. The experimental setup used in this study is a straight channel with a width of 0.40 m and a height of 0.50 m (Fig. 2). A collection channel with a width of 0.40 m and a height of 0.40 m is also mounted on the main channel (Fig. 2). The bottom slope of the main channel and the collection channel is 0.10%. The experiments were conducted for H-side weirs in a rectangular cross-sectional straight channel under steady flow conditions for the sub-critical regime. According to Novák and Cabelka (1981), surface tension effects are practical if the piezometric head over the weir is less than 3 cm. Therefore, all heads were taken larger than 3 cm, and thus, surface tension effects were neglected. Sieves were used as breakers and placed upstream of the main channel and toward the end of the collection channel to ensure stable flow conditions (i.e., unsteady flow).

While a digital flowmeter was used to measure Q total, a triangular V-notch weir was used for Q_c . A cross-sectional view of the experimental setup and flowchart of the present study is shown in Fig. 2.

As mentioned above, since the conducted the study of Ahmed (1985), several studies have been carried out. Since then, many researchers have investigated combined weirs and gates for frontal flows and introduced different combined weir–gate structures (Alhamid 1999; Alhamid et al. 1996; Altan-Sakarya and Kökpinar 2013; Negm et al. 2002; Negm 2002; Nouri and Hemmati 2020; Salehi and Azimi 2019; Samani and Mazaheri 2009; Severi et al. 2014).

Discharge of combined weir–gate, Q_c (Alhamid 1999; Alhamid et al. 1996; Altan-Sakarya and Kökpinar 2013; Ferro 2000; Negm et al. 2002; Negm 2002; Nouri and Hemmati 2020; Salehi and Azimi 2019; Samani and Mazaheri 2009; Severi et al. 2014) is:

$$Q_c = Q_g + Q_w \quad (5)$$

in which Q_g and Q_w are the discharge of the gate and weir (m^3/s), respectively.

Equation (6) uses lateral flows as the discharge equation for the under-gate flow (Ghodsian 2003; Swamee et al. 1993). However, Eq. (7) is the weir discharge equation for the Domínguez approach (Bagheri et al. 2014; Domínguez and Francisco 1959).

$$Q_g = C_{dg} a b_g \sqrt{2g y_1} \quad (6)$$

$$Q_w = \frac{4}{15} C_{dw} b_w \sqrt{2g} \left(\frac{h_2^{2.5} - h_1^{2.5}}{h_2 - h_1} \right) \quad (7)$$

If Eqs. (6) and (7) are substituted in Eq. (5). We will get Eq. (8)

$$Q_c = C_{dg} a b_g \sqrt{2g y_1} + \frac{4}{15} C_{dw} b_w \sqrt{2g} \left(\frac{h_2^{2.5} - h_1^{2.5}}{h_2 - h_1} \right) \quad (8)$$

Negm et al. (2002) and Altan-Sakarya and Kökpinar (2013) reported that applying the classical weir and gate discharge coefficient leads to intolerable mistakes in predicting the combined flow. Salehi and Azimi (2019) also said that interactions were between weir and gate flow. So, it results in excessive energy losses in the combined system. Consequently, using classical equations, the measured combined discharge differs from the calculated discharge separately for the weir and gates. Therefore, a different approach is necessary to estimate the discharge of the H-side weir rather than conventional equations. As stated above, an H-side weir is a system in which a side weir and a side gate are combined, as given in Fig. 1.



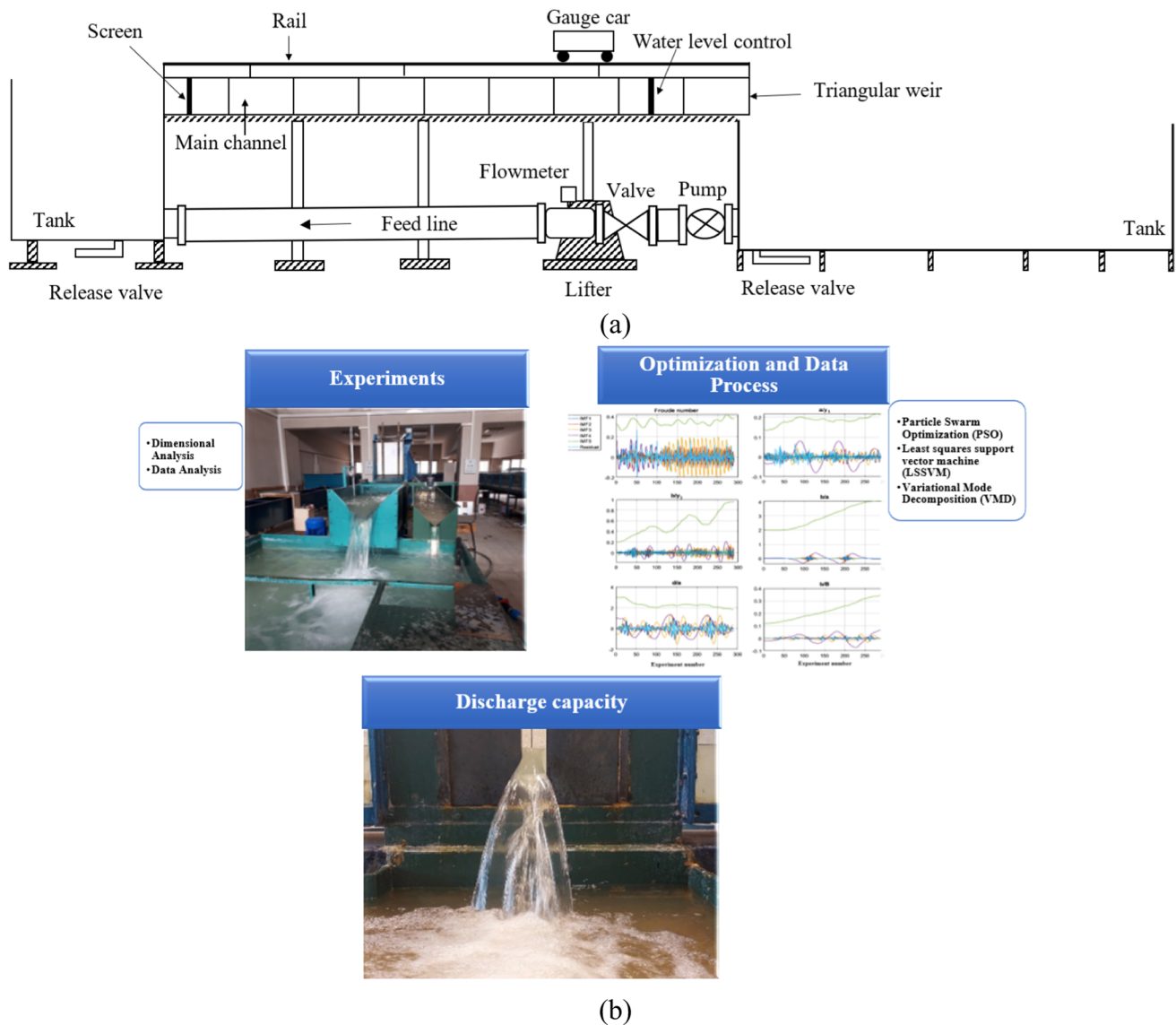


Fig. 2 Experimental setup and the flowchart of the present study

Dimensional analysis

The parameters affecting the H-side weir flow are presented in Eq. (9).

$$\Phi(Q_c, a, b, B, h, d, S_o, y_1, \varphi, \mu, \sigma, g, \rho) = 0 \quad (9)$$

where Q_c = discharge of H-side weir (m^3/s), a = gate opening (m), b ($b_w = b_g = b$) = length of the H-side weir (m), B = main channel width (m), h = head over the weir (m), d = vertical distance between the crest height of the weir and the top of the gate (m), S_o = main channel slope (-), y_1 = water depth at the upstream section of H-side weir (m), φ = deflection angle of the streamlines, σ = surface tension (kg/s^2), μ = dynamic

viscosity ($\text{kg}/\text{m s}$), g = gravitational acceleration (m/s^2) and ρ = mass density of the water (kg/m^3).

As a result, Eq. (10) is obtained (see “Appendix”).

$$\frac{Q_c}{b} \sqrt{ga^{1.5}} = f_1\left(\frac{y_1}{a}, \frac{b}{B}, \frac{b}{a}, \frac{h}{b}, \frac{d}{a}, F_1\right) \quad (10)$$

y_1/a and h/b are hydraulic parameters affecting the flow, and b/B , b/a and d/a are geometric parameters affecting the flow. Among the geometric parameters, d/a is called the obstruction ratio. Values and ranges of the physical and hydraulic conditions of the study are given in Table 1.



Least-squares support-vector machine (LSSVM)

The LSSVM algorithm is an enhanced version of SVM. For example, consider a given set of n data points $\{x_i, y_i\}$ where x_i is the i th input vector, and y_i is the corresponding output. Examples of a nonlinear mapping ϕ express the LSSVM algorithm as in Eq. (11).

$$f(x_i) = w^T \phi(x_i) + b \tag{11}$$

where w and b are the variables defined by minimizing.

The objective function:

$$R = \frac{1}{2}w^2 + \frac{1}{2}C \sum_{i=1}^N e_i^2 \tag{12}$$

where C is the regularization constant, and e_i is the training data error. Equation (3) is used to solve the optimization problem (Mellit et al. 2013; Suykens and Vandewalle 1999).

$$\begin{cases} \text{Minimize : } J(w, e_i) = \frac{1}{2}w^2 + \frac{1}{2}C \sum_{i=1}^N e_i^2 \\ \text{Subject to : } y_i = w^T(x_i) + b + e_i, i = 1, \dots, N \end{cases} \tag{13}$$

Particle swarm optimization (PSO)

PSO is an approach that tries to solve by mimicking the behavior of a flock of birds or fish. To find the most suitable solution, it tries to reach the best solution by updating the positions and velocities of the particles according to their neighbors. The PSO bio-inspired approach is a stochastic population-based technique. In this technique, the motion of each i in the search space is carried out by vectors as calculated in Eqs. (17) and (18).

$$v_i = \omega v_i + c_1 \eta_1 \circ (p_i - x_i) + c_2 \eta_2 \circ (g_{\text{best}} - x_i) \tag{14}$$

$$x_i = x_i + v_i \tag{15}$$

in which \circ : entry-wise products, $x_i, v_i, p_i, g_{\text{best}}$ values indicate position, velocity, best individual solution position and best neighbor solution position, respectively. In addition, c_1 and c_2 are acceleration constants, ω : inertia weight, η_1 and η_2 : random vectors (Katipoğlu and Sarıgöl 2023; Novoa-Hernández et al. 2011).

Variational mode decomposition (VMD)

VMD is a novel signal decomposition technique for separating a time series into various intrinsic mode functions and residuals. VMD is superior to wavelet transform and Hilbert–Huang transform because it has no modal aliasing effect and is sensitive to noise (Chaitanya et al. 2021; Sarıgöl and Katipoğlu 2023). This study aims to strengthen the VMD signal processing algorithm by integrating it into LSSVM.

Results and discussion

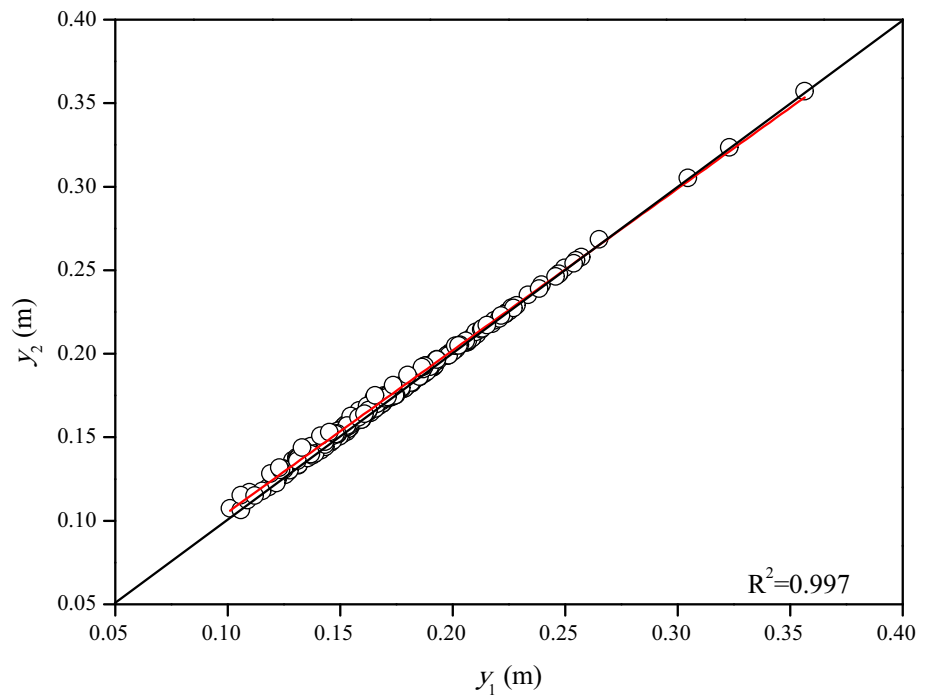
Experimental results

The variation of upstream and downstream flow depth is plotted in Fig. 3. Variations in specific energy at upstream and downstream sections in a straight channel in the H-side weir for the subcritical regime ($E_1 = y_1 + \frac{V_1^2}{2g}, E_2 = y_2 + \frac{V_2^2}{2g}$) are almost equal to each other and compatible with each other ($E_1 \cong E_2$). Similarly, upstream and downstream flow depths are almost equal to each other. Therefore, it is observed that the assumption of De Marchi (1934) and

Table 1 Physical and hydraulic conditions of the present study

	Parameters	Range and value
Main channel	Width, b (m)	0.40
	Height, z (m)	0.50
	Slope, S_0	0.001
H-side weir	Gate and weir length (m)	0.04–0.16
	Crest height, p (m)	0.06–0.09–0.12
	Total discharge, Q_1 (m ³ /s)	0.0095–0.046
	Upstream Froude number, F_1	0.06–0.93
	Head, h_1 (m)	0.034–0.266
	Vertical distance between the crest height of the weir and the top of the gate (m), d (m)	0.02–0.10
	Gate opening, a (m)	0.02–0.03–0.04
	Discharge of H-side weir, Q_c	0.0013–0.0189
	Upstream flow depth, y_1	0.101–0.357

Fig. 3 Variation of upstream and downstream flow depth



Domínguez and Francisco (1959) used to obtain the discharge coefficients for the gate and weir is correct, namely that the specific energy along the main channel is constant. As a result, specific energy at the upstream and downstream almost being equal to each other shows that De Marchi and Domínguez approaches can be safely used to study the H-side weir flow characteristics ($E_1 \cong E_2$).

Figure 4 shows the variation of d/y_1 with the parameter dimensionless unit discharge ($\frac{Q_c}{g^{0.5}a^{1.5}}$). When the figure is analyzed, it is seen that the geometry of the H-side weir is practical on the dimensionless unit discharge (q_t) value. The slope of the fitted line in Fig. 4 varies with increasing d/a value. The variation has a linear trend ($y = ax + b$) and a good agreement ($R^2 = 0.95\text{--}0.99$).

Figure 5 shows the variation of $\frac{Q_c}{g^{0.5}a^{1.5}}$ with the a/y_1 parameter. As demonstrated in Fig. 5, geometry effectively affects the dimensionless unit discharge value. The geometrical parameters (d/a and b/B) are shown in Fig. 5. Figure 5 demonstrates that the data can be scattered as different categories based on d/a . The variation of each category is clarified by the effects of geometrical parameters (d/a and b/B). The effect of the parameter d/a is thus significant because it allows discharge through the H-side weir. At a particular value of b/B , the discharge increases sharply as d/a increases. It can be related to increasing the head over the weir. For a particular a/y_1 , dimensionless unit discharge increases as d/a decreases. More fluctuations form at large lengths ($b/B > 0.2$) than at small lengths ($b/B < 0.2$). The deviation between the weir and gate jet trajectory is minimal at small Froude

numbers but increases with F_1 . The weir flow and the gate flow are in contact at large lengths ($b/B > 0.2$), but this does not appear at small lengths ($b/B < 0.2$) and high F_1 values. The weir flow is in contact with the gate flow, leading to a breaking of the energy of the gate flow, and this is particularly noticeable for small obstruction ratios (d/a). Therefore, hydraulic designers need to consider such situations when using the H-weir in lateral flows for purposes such as water intake and flow regulation.

Consequently, the total discharge through the H-side weir increases because the side gate flow is higher than that of the side weir flow for larger a . The slope of the fitted line increases with the decrease of d/a value. The smallest values for the variation of the dimensionless unit discharge with a/y_1 are obtained for $d/a = 0.50$. Their variation is a polynomial function ($y = ax^2 + bx + c$) with a good agreement ($R^2 = 0.99$).

Figure 6 demonstrates the variation of $\frac{Q_c}{g^{0.5}a^{1.5}}$ with the b/y_1 . As demonstrated in Fig. 6, the H-side weir geometry is practical on the dimensionless unit discharge value. The slope of the fitted line varies with the decrease of d/a value. Their relationship is a polynomial function ($y = ax^2 + bx + c$), and its coefficient of determination is 0.99.

Figure 7 shows the variation of $\frac{Q_c}{g^{0.5}a^{1.5}}$ with b/h_1 . Figure 7 shows that q_t increases with increasing b/a . As shown in Fig. 7, the value of b/a is quite effective on q_t . However, after a certain point ($b/h_1 = 2$), it has the same effect on the change between q_t and b/h_1 . It is observed that an exponential relationship can be fitted for this variation. The variation of q_t

Fig. 4 Variation of dimensionless unit discharge ($\frac{q_c}{g^{0.5}a^{1.5}}$) with d/y_1

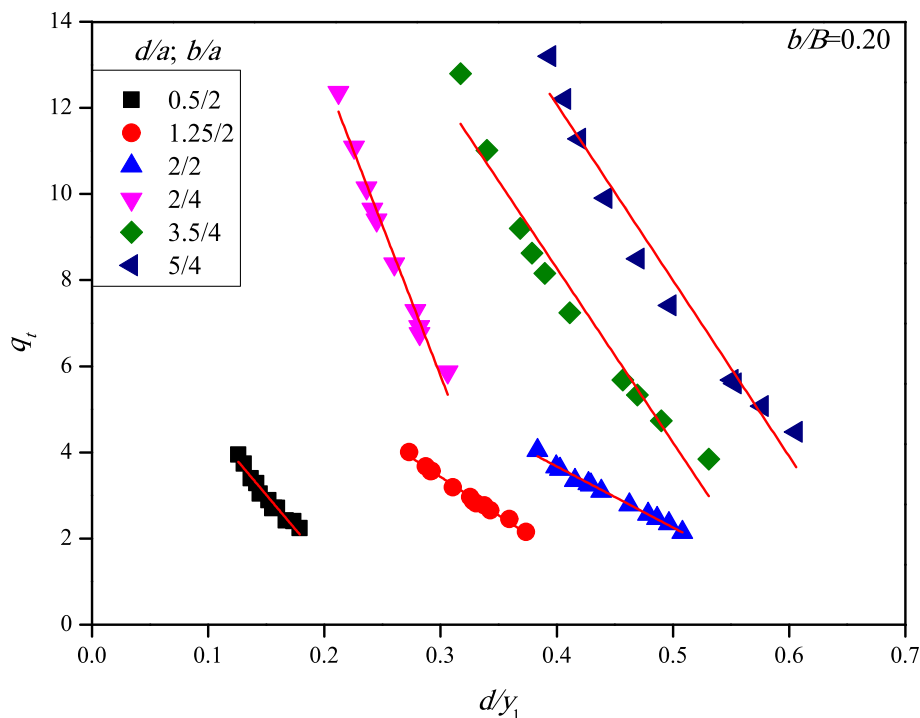
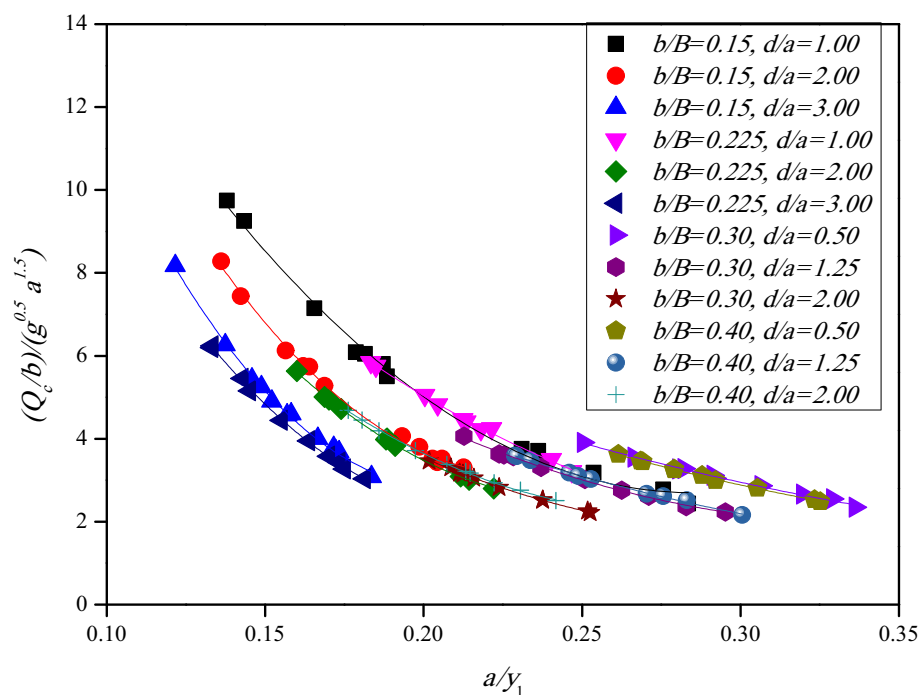


Fig. 5 Variation of q_t with a/y_1



with b/h_1 is an exponential function ($y = a + be^{cx}$). It is seen that the relationship with b/h_1 has good agreement ($R^2 = 0.99$).

A new equation was proposed for hydraulic designers to estimate the discharge capacity of an H-side weir ($\frac{q_c}{g^{0.5}a^{1.5}}$) using both hydraulic and geometrical parameters. The

contribution of a/y_1 , b/h_1 , b/B , F_1 and d/a to q_t is thus significant. As shown in Fig. 8, the measured and calculated values of q_t are compatible. Therefore, it can be reported that the proposed equation [Eq. (16)] is in good agreement. This equation was obtained using the least-squares error method ($R^2 = 0.995$) for H-side weir flow under $0 < F_1 < 1$ and $0.10 \leq b/B \leq 0.40$ and $0.50 \leq d/a \leq 5$ conditions.

Fig. 6 Variation of q_t with b/y_1

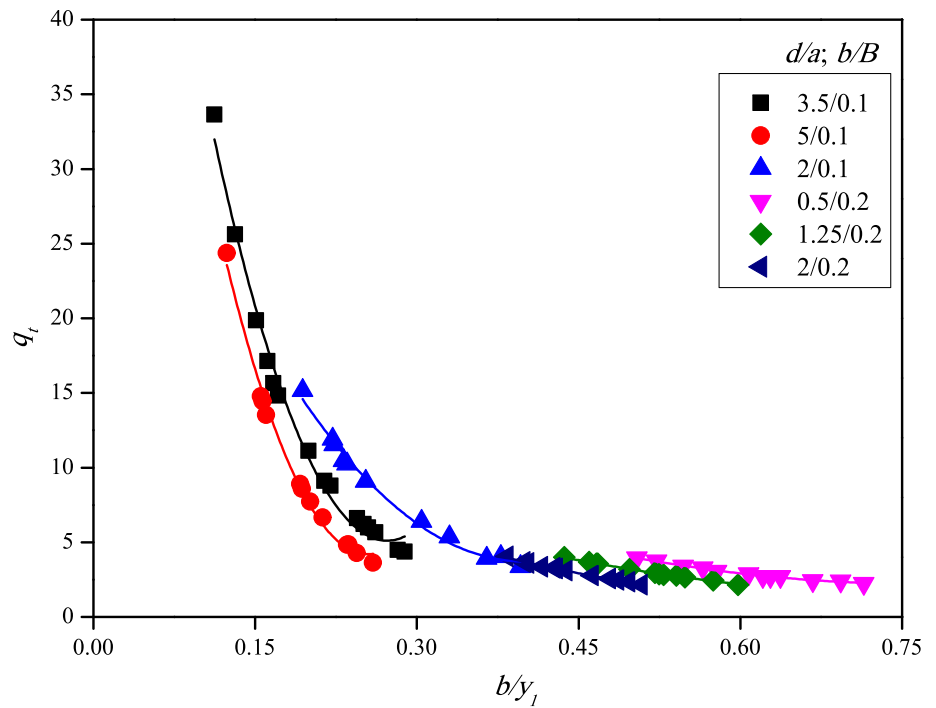
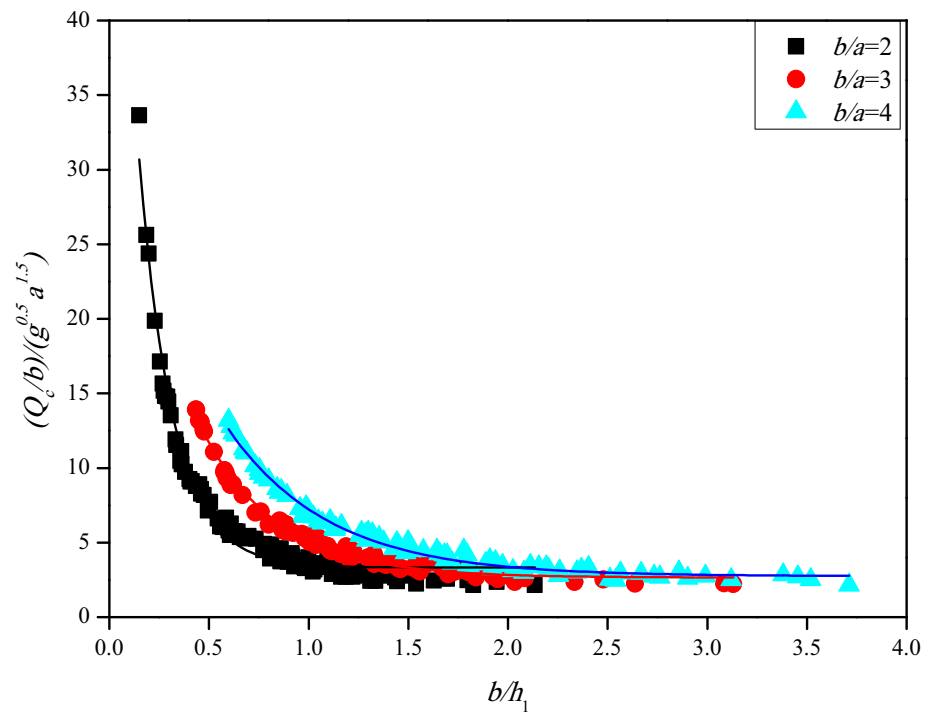


Fig. 7 Variation of q_t with b/y_1



$$q_t = 0.18F_1^{-0.04} \left(\frac{a}{y_1}\right)^{-2.56} \left(\frac{b}{y_1}\right)^{0.50} \left(\frac{b}{a}\right)^{-0.56} \left(\frac{d}{a}\right)^{-0.60} \left(\frac{b}{B}\right)^{-0.021094} \tag{16}$$

Figure 8 shows the comparison of the predicted and measured values of $\frac{Q_c}{g^{0.5} a^{1.5}}$. As demonstrated in Fig. 8, it is clear that the scatter data are compatible, i.e., there is a

perfect correlation between the measured and predicted values, and therefore, the equation is very reliable ($R^2=0.995$).

Figure 9 shows the interpretation of the residuals with measured values of $\frac{Q_c}{g^{0.5} a^{1.5}}$ at H-side weir. The figure shows tiny differences between the measured and predicted values. So, it can be stated that the study is reliable.

Fig. 8 Variation of measured and calculated q_t values

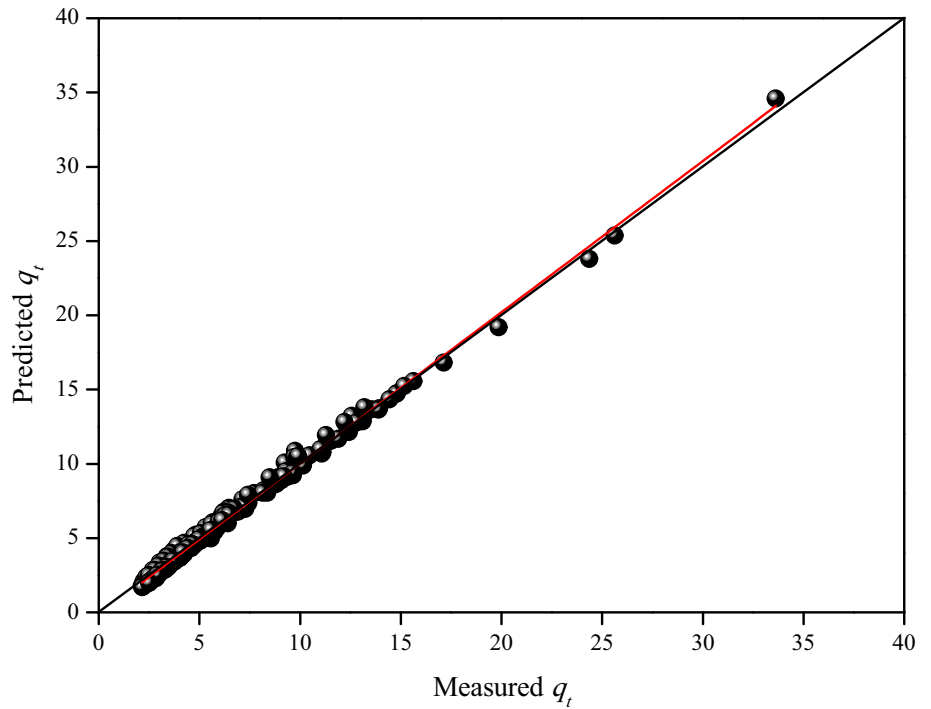


Figure 10 shows the variation of $\frac{Q_c}{g^{0.5}a^{1.5}}$ with F_1 . As shown in Fig. 10, q_t is large at small upstream Froude numbers (i.e., from $F_1 = 0.05$ to $F_1 = 0.20$). It is observed that after a certain value of F_1 (from $F_1 = 0.40$), q_t nearly remains the same.

Figure 11 shows the variation of q_t parameter with b/B . As shown in Fig. 11, b/B ratio affects the dimensionless unit discharge.

The interpretation of the discharge coefficient of the H-side weir with $\frac{Q_c}{g^{0.5}a^{1.5}}$ is plotted in Fig. 12. Generally, C_d increases logarithmic with increasing value of q_t . The discharge coefficient values range from around 0.50–0.68. The data in Fig. 12 are scattered due to the variation of the H-side weir models' geometrical parameters (d/a and b/a). It was observed that large discharge coefficient values are related to high b/a and d/a values and vice versa.

Fig. 9 Variation of residuals with q_t

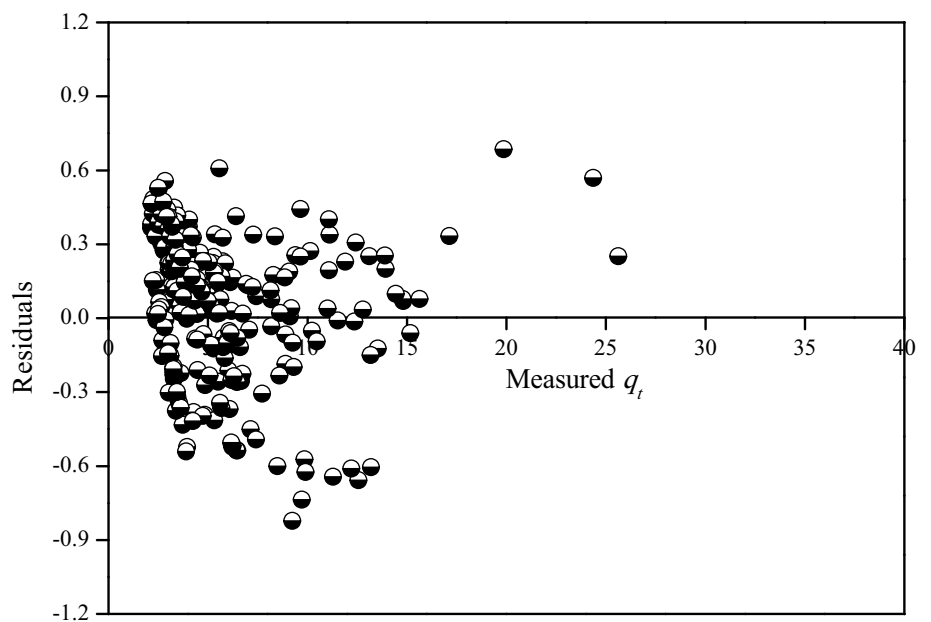


Fig. 10 Variation of q_t parameter with F_1

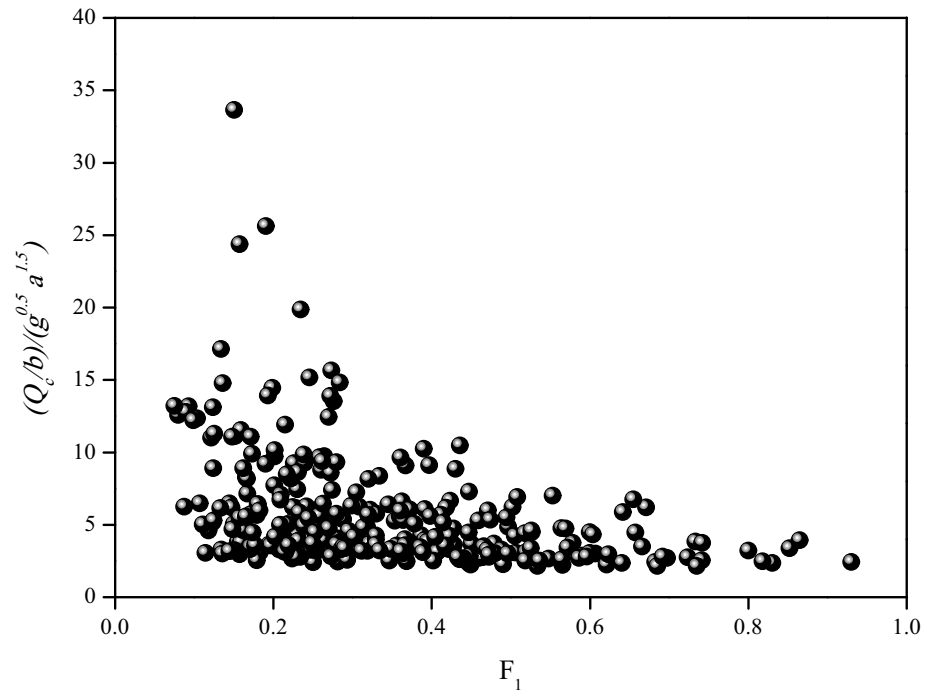
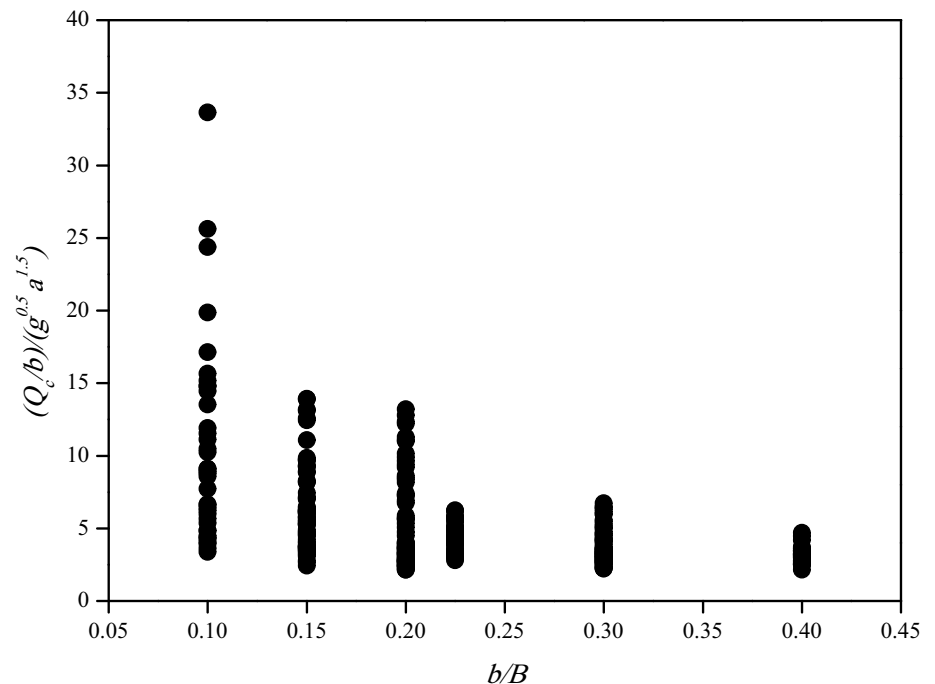


Fig. 11 Variation of q_t with b/B



The comparison of the present study with the literature is plotted in Fig. 13. The present study is compared with the studies of Negm et al. (2002) and Askeroglu (2006). They conducted their studies for frontal flows. However, the present study is conducted for lateral flow. Negm et al. (2002) stated that the study is valid for $0.47 \leq d/a \leq 4.00$, $0.65 \leq b/a \leq 5.00$, $1.80 \leq y_1/a \leq 7.50$ and $0 \leq S_0 \leq 0.0161$

for frontal flow. Moreover, Askeroglu (2006) stated that the study is valid for $1.34 \leq y_1/a \leq 8.30$, $0.25 \leq d/a \leq 4.40$, $0.06 \leq h/b \leq 2.08$, $2.50 \leq B/b \leq 6.00$, $1.00 \leq b/a \leq 2.50$ conditions. Although the flow type differs, the present study is compatible with Negm et al. (2002) and Askeroglu (2006). The present study was conducted for $0.10 \leq b/B \leq 0.40$, $0 < F_1 < 1$, $2 \leq b/a \leq 4$ and $0.50 \leq d/a \leq 5$. Trend of variation



Fig. 12 Variation of discharge coefficient with q_t

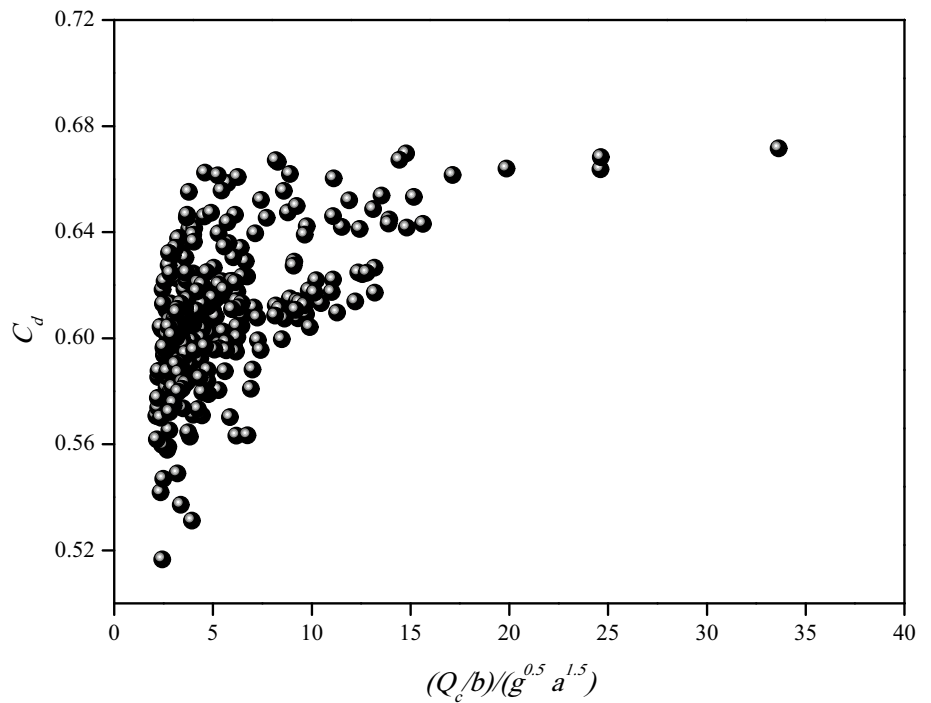
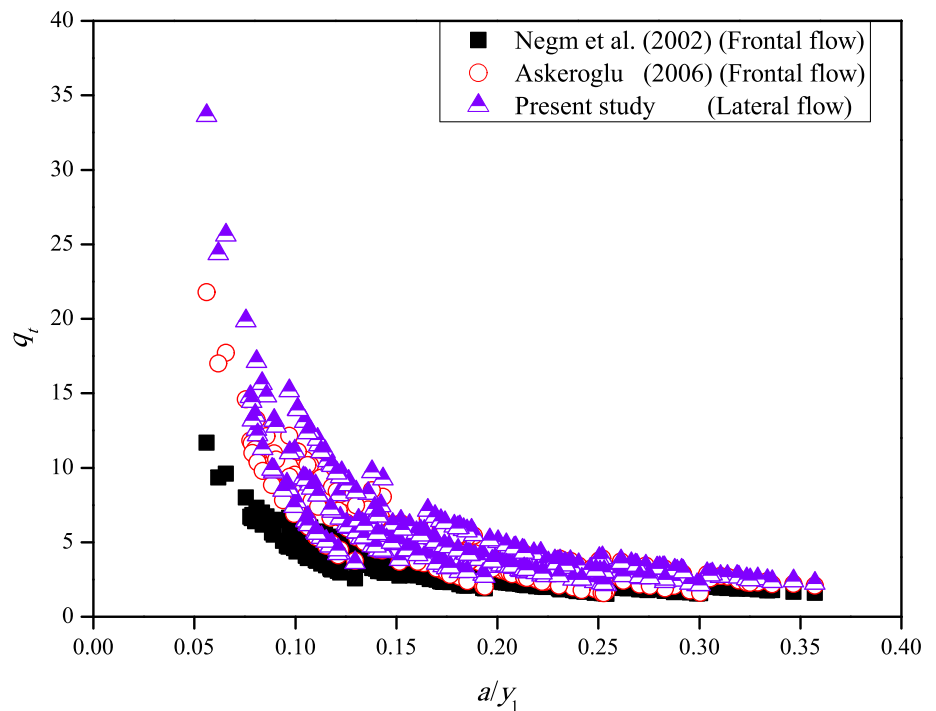


Fig. 13 Comparison of the present study with the literature



of q_t with a/y_1 is similar to the literature. The differences between q_t values can be due to different geometric (d/a , b/a and b/B) and hydraulic conditions (a/y_1 , b/y_1 , b/h_1 and d/y_1) and flow type.

Statistical values for the current study are given in Table 2. As shown in Table 2, the data have a good

agreement. Bias refers to a systematic deviation from the actual value. The root mean square errors (RMSE), average percent error (APE), mean absolute percentage errors (MAPE), scatter index (SI), BIAS and coefficient of determination (R^2) were calculated below.

Table 2 Statistical values of proposed Eq. (19)

RMSE	MAE	MAPE	SI	BIAS	R^2
0.30	0.25	5.84	0.0534	0.067	0.995

$$\text{RMSE} = \sqrt{\frac{1}{N} \sum_{i=1}^N (\text{Predicted}_i - \text{Observed}_i)^2} \quad (17)$$

$$\text{SI} = \frac{\text{RMSE}}{\bar{x}} \quad (18)$$

$$\text{BIAS} = \frac{1}{N} \sum_{i=1}^N (\text{Observed}_i - \text{Predicted}_i) \quad (19)$$

$$\text{MAE} = \frac{1}{N} \sum_{i=1}^N |\text{Observed}_i - \text{Predicted}_i| \quad (20)$$

$$\text{MAPE} = \frac{100}{N} \sum_{i=1}^N \left| \frac{\text{Observed}_i - \text{Predicted}_i}{\text{Observed}_i} \right| \quad (21)$$

in which N is the total number of runs, i is its run and \bar{x} is the mean value observed.

Moreover, Q_c increases with increasing b/a at constant $d/a=2$. For narrow range of d/a (i.e., $d/a=0.5$ and 1), little variations are observed; for a wide range of y/d (i.e., $d/a=2$ and 5), high variations of Q_c with a/y_1 are observed. The decreasing trend of the change between a/y_1 and Q_c decreases with the increase of b/a . For instance, the slope line is 0.1041 for $b/a=4$ but 0.0612 for $b/a=2$. The slope line decreases by 41.2% with the decrease of b/a . The variation has a linear trend ($y=ax+b$), and the coefficient of determination is from 0.95 to 0.99. The trend of the change between d/y_1 and Q_c increases with the increase of b/a . For instance, the slope of the line is 0.0297 for $b/a=4$ and 0.031 for $b/a=2$. The slope line increases by 4.4% with the increase of b/a . The variation is a linear trend ($y=ax+b$), and the coefficient of determination is from 0.95 to 0.99. Moreover, the discharge capacity of the H-side weir is 1.3–4 times higher than conventional side weirs and 1.6–9.0 times higher than side gates under the same conditions.

LSSVM, PSO and VMD results

Moreover, the study aims to estimate the H-side weir discharge capacity by combining various artificial intelligence, bio-inspired optimization and data decomposition techniques using geometrical parameters (d/a) and flow parameters. Furthermore, least-squares support-vector

machines (LSSVM), particle swarm optimization (PSO) and variable mode decomposition (VMD) algorithms are combined. This study selected 70% of the data for training and 30% for testing in setting up the prediction model. PSO updates particle velocities and positions using global best result (g_{best}) values and p_{best} , and the search process ends when the maximum number of iterations is reached. PSO was applied with 300 iterations. Different experiments were conducted as the number of particles (N) and c constants varied depending on the problem to be solved. Therefore, $N=20$ and $c_1=c_2=2$ values were selected as they yielded very prosperous results. The SVM model was set up using a radial basis kernel function.

Experimental data used to estimate the H-side weir discharge capacity were sub-banded by VMD. VMD-LSSVM and PSO-VMD-LSSVM hybrid models were established by presenting them as inputs to such LSSVM and PSO-LSSVM models in Fig. 14.

Taylor diagrams are used to evaluate the performance of the artificial intelligence models established in the H-side weir capacity estimation in Fig. 15. Taylor diagrams are widely used to visualize the similarities and relationships between time series. Accordingly, during the training phase, the VMD-LSSVM hybrid approach with the highest correlation coefficient (R) and the lowest root mean square error (RMSE) value showed the most accurate estimation results. In addition, the fact that this model is closest to the actual data and has the same standard deviation value supports the predictive success of the model. In the testing phase, it was concluded that the PSO-LSSVM model was the best model with the lowest R and highest RMSE values. In addition, it is noteworthy that all models' predictions are promising and satisfactory.

Boxplot graphics were used during the training phase to evaluate the H-side weir discharge capacity estimates in Fig. 16. These graphs visually select the most suitable model by comparing the actual data's spread, distribution, percentiles and outliers with the artificial intelligence prediction results. According to this, it is deduced that the properties are the most suitable for the actual data and the LSSVM and VMD-LSSVM models because their structures are similar.

Boxplot plots were used in the testing phase to compare the estimation results of the H-side weir discharge capacity in Fig. 17. Accordingly, the PSO-LSSVM model shows the most compatible distribution with the actual data. It is also noteworthy that the structure of the PSO-VMD-LSSVM models is quite similar to the actual data.

The success of the hybrid estimation models of H-side weir discharge capacity was compared based on various statistical indicators in Table 3. The optimum model was indicated to have the lowest error, Bias factor closest to 1 and highest determination coefficient value (R^2). Therefore, statistical indicators were ranked to determine



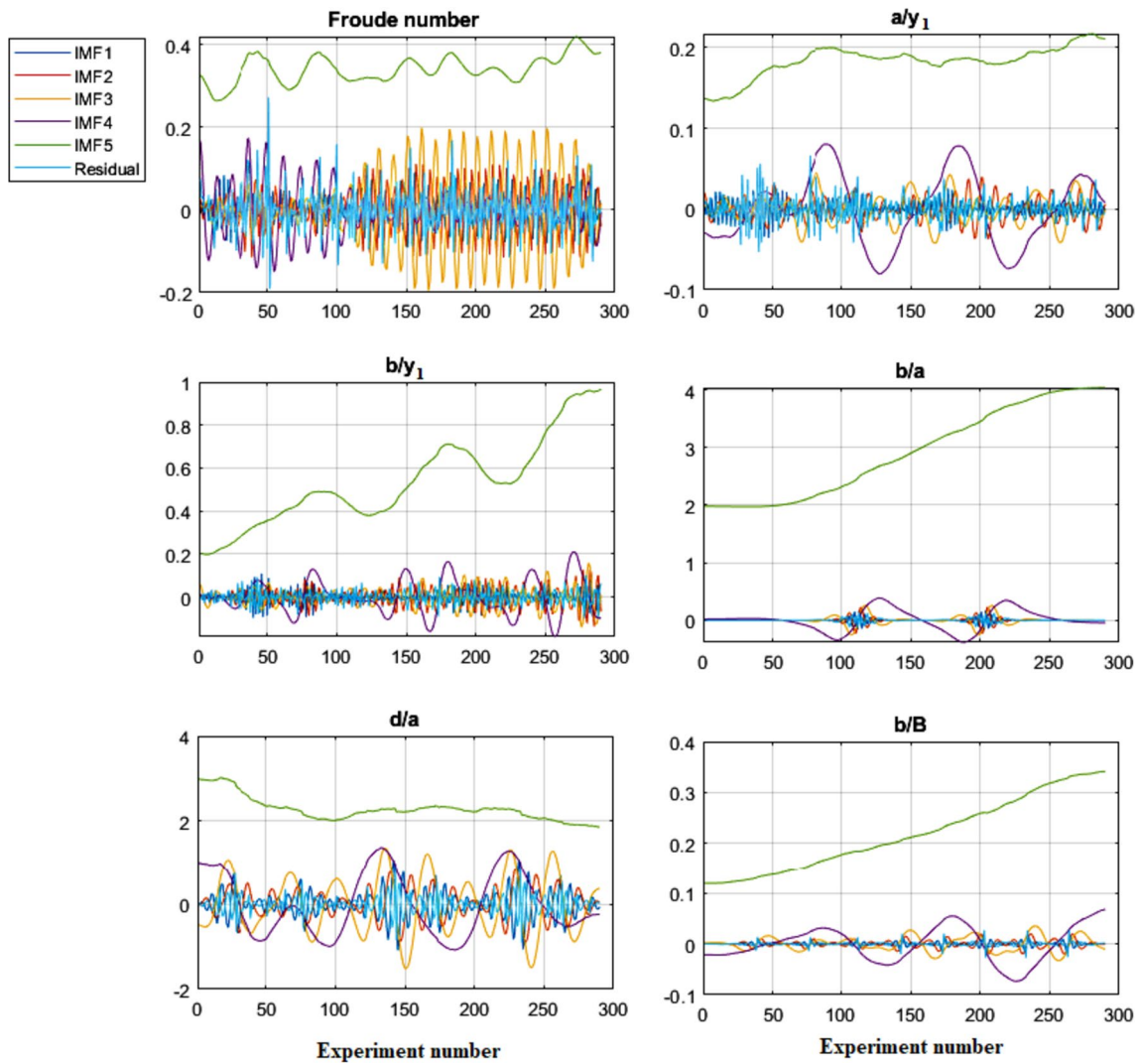


Fig. 14 Separation of experimental data used in the study into sub-bands with VMD

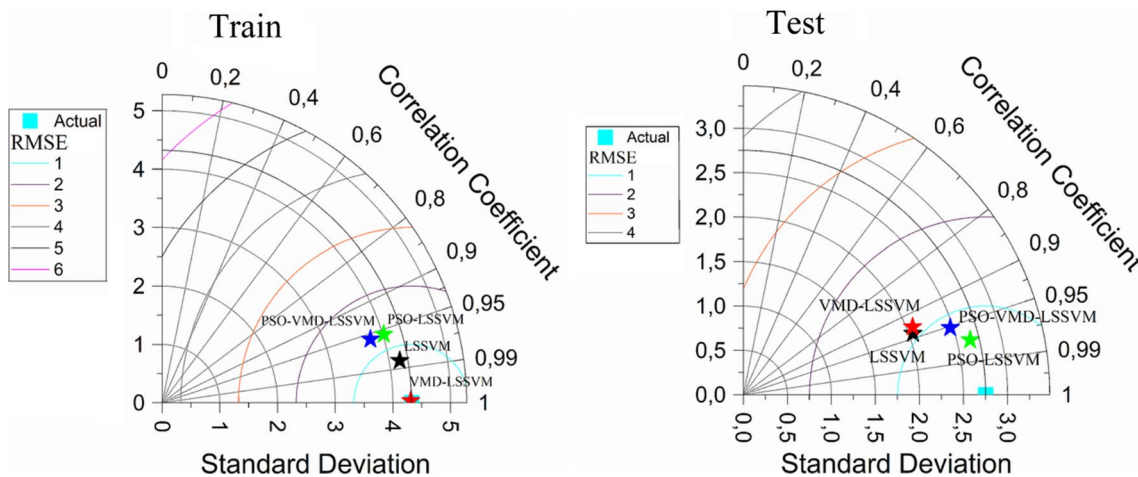


Fig. 15 Comparison of H-side weir discharge capacity estimation models with Taylor diagram

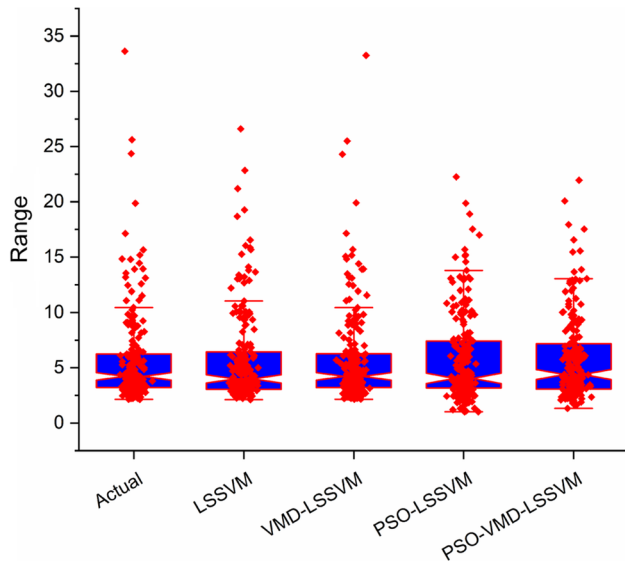


Fig. 16 Comparing the accuracy of the prediction models in the training phase with Boxplot plots

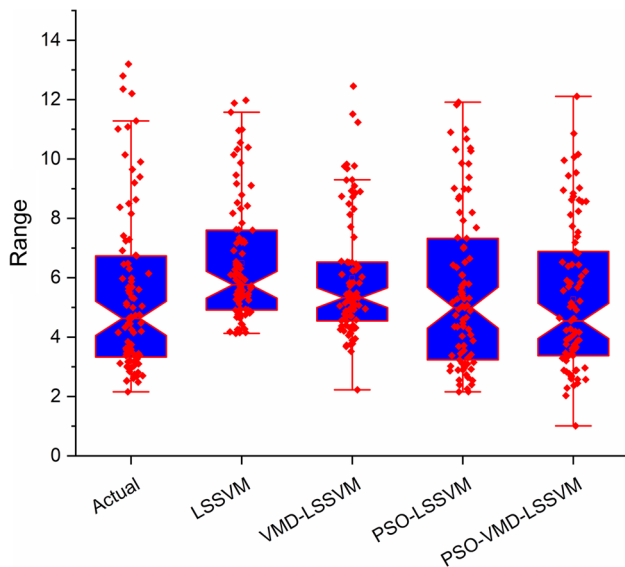


Fig. 17 Comparing the accuracy of the prediction models in the test phase with Boxplot plots

the optimum model, with the highest rank value indicating the best model. Accordingly, the success ranking of the models was presented as VMD-LSSVM > PSO-LSSVM > PSO-VMD-LSSVM > LSSVM.

Conclusion

In this study, the flow characteristics of H-side weirs were investigated in detail for free-flow conditions and subcritical flow regimes in a straight channel. The discharge capacity of the H-side weir is 1.3–4.0 times higher than conventional side weirs and 1.6–9.0 times higher than side gates under the same conditions. The side flow breaks the gate flow in low d/a values, while the side flow does not contact the gate flow and thus does not break the gate flow. The geometrical parameter (d/a) and the flow parameters (a/y_1 , h/b and F_1) significantly affect discharge capacity, while the others are negligible. Therefore, a discharge equation was proposed using a/y_1 , h/b , b/B , F_1 and d/a with a mean absolute percentage error (MAPE) of about 5.84%. The success ranking of the models was presented as VMD-LSSVM > PSO-LSSVM > PSO-VMD-LSSVM > LSSVM. It was concluded that the PSO-LSSVM model was the best model with the lowest R and highest RMSE values in the testing phase. The developed equation [Eq. (16)] is compatible with observations within the limitations of the present experimental work. Moreover, the most successful model for estimating the H-side weir discharge capacity values was VMD-LSSVM based on statistical analyses. In addition, it was concluded that the established LSSVM, PSO-LSSVM and PSO-VMD-LSSVM models produced very satisfactory predictions.

Appendix

The parameters affecting the H-side weir flow are presented in Eq. (9).

$$\Phi(Q_c, a, b, B, h, d, S_0, y_1, \varphi, \mu, \sigma, g, \rho) = 0 \quad (9)$$

where Q_c = discharge of H-side weir (m^3/s), a = gate opening (m), b ($b_w = b_g = b$) = length of the H-side weir (m), B = main channel width (m), h = head over the weir (m), d = vertical distance between the crest height of the weir and the top of the gate (m), S_0 = main channel slope (–), y_1 = water depth at the upstream section of H-side weir (m), φ = deflection angle of the streamlines, σ = surface tension (kg/s^2), μ = dynamic viscosity ($\text{kg}/\text{m s}$), g = gravitational acceleration (m/s^2) and ρ = mass density of the water (kg/m^3).

The main channel width, flow depth and Froude number are effective on the value of φ . As suggested by Subramanya and Awasthy (1972), φ is neglected in the dimensional analysis [Eq. (10)] because these variables are taken into account. If the equation is rearranged:

$$\Phi(Q_c, a, b, B, h, d, S_0, y_1, \mu, \sigma, g, \rho) = 0 \quad (22)$$

Buckingham's Theory is used for dimensional analysis. Gravitational acceleration (g), mass density (ρ) and gate

Table 3 Testing the accuracy of the established hybrid prediction models according to various statistical indicators

	MSE	MAE	MAPE	MBE	Bias factor	R ²	Total Rank
<i>LSSVM</i>							
Train	0.565	0.38	0.063	0	0.998	0.963	53
Rank	6	7	7	8	7	7	
Test	2.223	1.181	0.328	1.039	1.316	0.887	
Rank	1	1	1	5	1	2	
<i>VMD-LSSVM*</i>							
Train	0.001	0.016	0.003	0	1	1	65
Rank	8	8	8	8	8	8	
Test	1.542	0.986	0.239	0.531	1.192	0.863	
Rank	4	2	2	6	2	1	
<i>PSO-LSSVM</i>							
Train	1.604	0.727	0.144	0	0.992	0.901	62
Rank	3	3	3	8	6	4	
Test	0.414	0.480	0.091	0.081	1.021	0.946	
Rank	7	6	6	7	3	6	
<i>PSO-VMD-LSSVM</i>							
Train	1.687	0.653	0.109	0	1.013	0.900	54
Rank	2	4	5	8	4	3	
Test	0.756	0.622	0.136	-0.181	0.988	0.906	
Rank	5	5	4	4	5	5	

*Indicates the optimum model

opening (*a*) are selected as repeated variables. The details of the dimensional analysis are below:

$$\Pi_1 = \rho^{x_1} g^{y_1} a^{z_1} Q_c$$

$$M^0 = 1x_1 + 0y_1 + 0z_1 + 0 = 0$$

$$L^0 = -3x_1 + 1y_1 + 1z_1 + 3 = 0$$

$$T^0 = 0x_1 - 2y_1 + 0z_1 - 1 = 0$$

$$x_1 = 0, y_1 = -\frac{5}{2}, z_1 = -\frac{1}{2}$$

$$\Pi_1 = \rho^0 g^{-1/2} a^{-5/2} Q_c = \frac{Q_c}{\sqrt{g} a^{2.5}}$$

$$\Pi_2 = \rho^{x_2} g^{y_2} a^{z_2} \mu$$

$$M^0 = 1x_2 + 0y_2 + 0z_2 + 1 = 0$$

$$L^0 = -3x_2 + 1y_2 + 1z_2 - 1 = 0$$

$$T^0 = 0x_2 - 2y_2 + 0z_2 - 1 = 0$$

$$x_2 = -1, y_2 = -\frac{1}{2}, z_2 = -\frac{3}{2}$$

$$\Pi_2 = \rho^{-1} g^{-1/2} a^{-3/2} \mu = \frac{\mu}{\sqrt{g} a^{1.5} \rho} = \frac{\nu}{\sqrt{g} a^{1.5}}$$

$$\Pi_3 = \rho^{x_3} g^{y_3} a^{z_3} b$$

$$M^0 = 1x_3 + 0y_3 + 0z_3 + 0 = 0$$

$$L^0 = -3x_3 + 1y_3 + 1z_3 + 1 = 0$$

$$T^0 = 0x_3 - 2y_3 + 0z_3 + 0 = 0$$

$$x_3 = 0, y_3 = 0, z_3 = -1$$

$$\Pi_3 = \rho^0 g^0 a^{-1} b = \frac{b}{a}$$

$$\Pi_4 = \frac{B}{a}$$



$$\Pi_5 = \frac{y_1}{a}$$

$$\Pi_6 = \frac{h}{a}$$

$$\Pi_7 = \frac{d}{a}$$

$$\Pi_8 = \rho^{x_8} g^{y_8} a^{z_8} S_0$$

$$M^0 = 1x_8 + 0y_8 + 0z_8 + 0 = 0$$

$$L^0 = -3x_8 + 1y_8 + 1z_8 + 0 = 0$$

$$T^0 = 0x_8 - 2y_8 + 0z_8 + 0 = 0$$

$$x_8 = 0, y_8 = 0, z_8 = 0$$

$$\Pi_8 = \rho^0 g^0 a^0 S_0 = S_0$$

$$\Pi_9 = \rho^{x_9} g^{y_9} a^{z_9} \sigma$$

$$M^0 = 1x_9 + 0y_9 + 0z_9 + 1 = 0$$

$$L^0 = -3x_9 + 1y_9 + 1z_9 + 0 = 0$$

$$T^0 = 0x_9 - 2y_9 + 0z_9 - 2 = 0$$

$$x_9 = -1, y_9 = -1, z_9 = -2$$

$$\Pi_9 = \rho^{-1} g^{-1} a^{-2} \sigma = \frac{\sigma}{\rho g a^2}$$

$$F_1 = \frac{\Pi_1}{\Pi_4 \Pi_5}$$

$$\text{Re} = \frac{\Pi_1}{\Pi_2 \Pi_6}$$

$$\text{We} = \frac{\Pi_1^2}{\Pi_9 \Pi_4^2}$$

$$\frac{\Pi_3}{\Pi_4} = b/B$$

$$\frac{\Pi_3}{\Pi_6} = b/h$$

$$q_t = \frac{\Pi_1}{\Pi_3} = \frac{Q_c/b}{\sqrt{g} a^{1.5}}$$

$$\Phi \left(\frac{\frac{Q_c}{b}}{\sqrt{g} a^{1.5}}, \frac{y_1}{a}, \frac{b}{B}, \frac{b}{a}, \frac{h}{b}, \frac{d}{a}, \text{Re}, F_1, \text{We}, S_0 \right) = 0 \quad (23)$$

The piezometric head over the weir was taken larger than 3 cm as suggested by Novák and Cabelka (1981), and therefore, the effect of surface tension was neglected. The effect of S_0 is neglected since the bottom slope of the channel is constant for each model used in the experiments (Askeroğlu 2006; Borghei et al. 1999). Re is neglected since the effect of viscous effects is negligible in turbulent flow conditions (Askeroğlu 2006; Henderson 1966). If necessary adjustments are made, Eq. (24) is obtained.

$$\Phi \left(\frac{\frac{Q_c}{b}}{\sqrt{g} a^{1.5}}, \frac{y_1}{a}, \frac{b}{B}, \frac{b}{a}, \frac{h}{b}, \frac{d}{a}, F_1 \right) = 0 \quad (24)$$

If Eq. (24) is rearranged:

$$\frac{\frac{Q_c}{b}}{\sqrt{g} a^{1.5}} = f_1 \left(\frac{y_1}{a}, \frac{b}{B}, \frac{b}{a}, \frac{h}{b}, \frac{d}{a}, F_1 \right) \quad (10)$$

Funding There is no funding source.

Data availability Upon to reasonable request.

Declarations

Conflict of interest The authors declare that they have no conflict of interest.

References

- Ahmed FH (1985) Characteristics of discharge of combined flow through sluice gate and over weirs. *J Eng Technol Iraq* 3(2):49–65
- Al-Bedyry NK, Kadim MAA, Hussein SH, Al-Khafaji ZS, Al-Husseinawi FN (2023) Experimental establishing of moving hydraulic jump in a trapezoidal channel. *Civ Eng J (iran)* 9(4):873–881. <https://doi.org/10.28991/CEJ-2023-09-04-08>
- Alhamid AA (1999) Analysis and formulation of flow through combined V-notch-gate-device. *J Hydraul Res* 37(5):697–705. <https://doi.org/10.1080/00221689909498524>
- Alhamid AA, Husain D, Negm AAM (1996) Discharge equation for simultaneous flow over rectangular weirs and below inverted triangular weirs. *Arab Gulf J Sci Res* 14(3):595–607



- Alhamid AA, Negm AAM, Al-Brahim AM (1997) Discharge equation for proposed self-cleaning device. *J King Saud Univ – Eng Sci* 9(1):13–23. [https://doi.org/10.1016/S1018-3639\(18\)30664-0](https://doi.org/10.1016/S1018-3639(18)30664-0)
- Altan-Sakarya AB, Kökpinar MA (2013) Computation of discharge for simultaneous flow over weirs and below gates (H-weirs). *Flow Meas Instrum* 29:32–38. <https://doi.org/10.1016/j.flowmeasinst.2012.09.007>
- Altan-Sakarya AB, Kökpinar MA, Duru A (2020) Numerical modeling of contracted sharp-crested weirs and combined weir and gate systems. *Irrig Drain*. <https://doi.org/10.1002/ird.2468>
- Ayaz M, Chourasiya S, Danish M (2023) Performance analysis of different ANN modelling techniques in discharge prediction of circular side orifice. *Model Earth Syst Environ*. <https://doi.org/10.1007/s40808-023-01766-7>
- Azamatulla HM, Emamgholizadeh S, Parsaie A, Haghiabi AH (2019) Prediction of discharge coefficient of combined weir-gate using ANN, ANFIS and SVM. *Int J Hydrol Sci Technol* 9(4):412–430. <https://doi.org/10.1504/ijhst.2019.10024040>
- Bagheri S, Kabiri-Samani AR, Heidarpour M (2014) Discharge coefficient of rectangular sharp-crested side weirs Part II: Domínguez's method. *Flow Meas Instrum* 35:116–121. <https://doi.org/10.1016/j.flowmeasinst.2013.10.006>
- Balouchi B, Rakhshandehroo G (2018) Using physical and soft computing models to evaluate discharge coefficient for combined weir-gate structures under free flow conditions. *Iran J Sci Technol - Trans Civ Eng* 42(4):427–438. <https://doi.org/10.1007/s40996-018-0117-0>
- Bonakdari H, Zaji AH (2018) New type side weir discharge coefficient simulation using three novel hybrid adaptive neuro-fuzzy inference systems. *Appl Water Sci* 8(1):1–15. <https://doi.org/10.1007/s13201-018-0669-y>
- Borgei SM, Jalili MR, Ghodsian M (1999) Discharge coefficient for sharp-crested side weir in subcritical flow. *J Hydraul Eng* 125(10):1051–1056
- Chaitanya BK, Yadav A, Pazoki M, Abdelaziz AY (2021) A comprehensive review of islanding detection methods. In: Ahmed SHEAA, Zobaa F (eds) *Uncertainties in modern power systems*. Academic Press, Cambridge, pp 211–216
- Chen W, Sharifrazi D, Liang G, Band SS, Chau KW, Mosavi A (2022) Accurate discharge coefficient prediction of streamlined weirs by coupling linear regression and deep convolutional gated recurrent unit. *Eng Appl Comput Fluid Mech* 16(1):965–976. <https://doi.org/10.1080/19942060.2022.2053786>
- De Marchi G (1934) Essay on the performance of lateral weirs. *L' Energia Electtr*, Milan 11:849–860
- El Baradei SA, Abodonya A, Hazem N, Ahmed Z, El Sharawy M, Abdelghaly M, Nabil H (2022) Ethiopian dam optimum hydraulic operating conditions to reduce unfavorable impacts on downstream countries. *Civ Eng J (iran)* 8(9):1906–1919
- Elshaarawy MK, Hamed AK (2024) Predicting discharge coefficient of triangular side orifice using ANN and GEP models. *Water Sci* 38(1):1–20. <https://doi.org/10.1080/23570008.2023.2290301>
- Ferro V (2000) Simultaneous flow over and under a gate. *J Irrig Drain Eng* 126:190–193. [https://doi.org/10.1061/\(asce\)0733-9437\(2001\)127:5\(325\)](https://doi.org/10.1061/(asce)0733-9437(2001)127:5(325))
- Ghodsian M (2003) Flow through side sluice gate. *J Irrig Drain Eng* 129:458–463. [https://doi.org/10.1061/\(asce\)0733-9437\(2003\)129:6\(458\)](https://doi.org/10.1061/(asce)0733-9437(2003)129:6(458))
- Ghodsian M, Feyzollahi F, Ghodsian M (2020) Flow through side-combined structure in a channel bend under subcritical flow regime. *ISH J Hydraul Eng*. <https://doi.org/10.1080/09715010.2020.1861487>
- Henderson FM (1966) Open channel flow. *J Fluid Mech* 29(2):414–415
- Ismael AA, Suleiman SJ, Al-Nima RRO, Al-Ansari N (2021) Predicting the discharge coefficient of oblique cylindrical weir using neural network techniques. *Arab J Geosci*. <https://doi.org/10.1007/s12517-021-07911-9>
- Kartal V, Emiroglu ME (2022) Experimental analysis of combined side weir-gate located on a straight channel. *Flow Meas Instrum* 88(September):102250. <https://doi.org/10.1016/j.flowmeasinst.2022.102250>
- Katipoğlu OM, Sarıgöl M (2023) Coupling machine learning with signal process techniques and particle swarm optimization for forecasting flood routing calculations in the Eastern Black Sea Basin, Türkiye. *Environ Sci Pollut Res*. <https://doi.org/10.1007/s11356-023-25496-6>
- Li S, Shen G, Parsaie A, Li G, Cao D (2023) Discharge modeling and characteristic analysis of semi-circular side weir based on the soft computing method. *J Hydroinf*. <https://doi.org/10.2166/hydro.2023.268>
- Mellit A, Pavan AM, Benghanem M (2013) Least squares support vector machine for short-term prediction of meteorological time series. *Theoret Appl Climatol* 111(1–2):297–307. <https://doi.org/10.1007/s00704-012-0661-7>
- Negm AAM, Al-Brahim AM, Alhamid AA (2002) Combined-free flow over weirs and below gates. *J Hydraul Res* 40(3):359–365. <https://doi.org/10.1080/00221680209499950>
- Norouzi R, Daneshfaraz R, Ghaderi A (2019) Investigation of discharge coefficient of trapezoidal labyrinth weirs using artificial neural networks and support vector machines. *Appl Water Sci* 9(7):1–10. <https://doi.org/10.1007/s13201-019-1026-5>
- Nouri M, Hemmati M (2020) Discharge coefficient in the combined weir-gate structure. *Flow Meas Instrum* 75:1–11. <https://doi.org/10.1016/j.flowmeasinst.2020.101780>
- Novák P, Cabelka J (1981) *Models in hydraulic engineering; physical principles and design applications*. Pitman Advanced Publishing Program, Lanham
- Novoa-Hernández P, Corona CC, Pelta DA (2011) Efficient multi-swarm PSO algorithms for dynamic environments. *Memet Comput* 3(3):163–174. <https://doi.org/10.1007/s12293-011-0066-7>
- Parsaie A (2016) Predictive modeling the side weir discharge coefficient using neural network. *Model Earth Syst Environ* 2(2):1–11. <https://doi.org/10.1007/s40808-016-0123-9>
- Parsaie A, Haghiabi AH (2016) Prediction of discharge coefficient of side weir using adaptive neuro-fuzzy inference system. *Sustain Water Resour Manag* 2(3):257–264. <https://doi.org/10.1007/s40899-016-0055-6>
- Parsaie A, Haghiabi AH (2021) Mathematical expression for discharge coefficient of Weir-Gate using soft computing techniques. *J Appl Water Res* 9(3):175–183
- Parsaie A, Haghiabi AH, Saneie M, Torabi H (2017) Prediction of discharge coefficient of cylindrical weir-gate using adaptive neuro fuzzy inference systems (ANFIS). *Front Struct Civ Eng* 11(1):111–122. <https://doi.org/10.1007/s11709-016-0354-x>
- Parsaie A, Azamatulla HM, Haghiabi AH (2018) Prediction of discharge coefficient of cylindrical weir-gate using GMDH-PSO. *ISH J Hydraul Eng* 24(2):116–123. <https://doi.org/10.1080/09715010.2017.1372226>
- Parsaie A, Dehdar-Behbahani S, Chadee AA, Haghiabi AH (2023) Estimating the energy dissipation of flow passing over triangular and trapezoidal plan weirs using the GMDH model. *Water Pract Technol* 18(5):1115–1124. <https://doi.org/10.2166/wpt.2023.073>
- Qasim RM, Mohammed AA, Abdulhussein IA (2022) An investigating of the impact of bed flume discordance on the weir-gate hydraulic structure. *HighTech Innov J* 3(3):341–355. <https://doi.org/10.28991/HIJ-2022-03-03-09>
- Razmi M, Saneie M, Basirat S (2022) Estimating discharge coefficient of side weirs in trapezoidal and rectangular flumes using outlier robust extreme learning machine. *Appl Water Sci* 12(8):1–15. <https://doi.org/10.1007/s13201-022-01698-0>



- Roushangar K, Alami MT, Shiri J, Asl MM (2018) Determining discharge coefficient of labyrinth and arced labyrinth weirs using support vector machine. *Hydrol Res* 49(3):924–938. <https://doi.org/10.2166/nh.2017.214>
- Salehi S, Azimi AH (2019) Discharge characteristics of weir-orifice and weir-gate structures. *J Irrig Drain Eng* 145(11):04019025. [https://doi.org/10.1061/\(asce\)ir.1943-4774.0001421](https://doi.org/10.1061/(asce)ir.1943-4774.0001421)
- Salmasi F, Nouri M, Sihag P, Abraham J (2021) Application of SVM, ANN, GRNN, RF, GP and RT models for predicting discharge coefficients of oblique sluice gates using experimental data. *Water Sci Technol: Water Supply* 21(1):232–248. <https://doi.org/10.2166/ws.2020.226>
- Samani JM, Mazaheri M (2009) Combined flow over weir and under gate. *J Hydraul Eng* 135:224–227. [https://doi.org/10.1061/\(asce\)0733-9429\(2009\)135:3\(224\)](https://doi.org/10.1061/(asce)0733-9429(2009)135:3(224))
- Sarıgöl M, Katipoğlu OM (2023) Estimation of monthly evaporation values using gradient boosting machines and mode decomposition techniques in the Southeast Anatolia Project (GAP) area in Turkey. *Acta Geophys*. <https://doi.org/10.1007/s11600-023-01067-8>
- Severi A, Masoudian M, Kordi E, Roettcher K (2014) Discharge coefficient of combined-free over-under flow on a cylindrical weir-gate. *ISH J Hydraul Eng*. <https://doi.org/10.1080/09715010.2014.939503>
- Seyedian SM, Haghiabi AH, Parsaie A (2023) Reliable prediction of the discharge coefficient of triangular labyrinth weir based on soft computing techniques. *Flow Meas Instrum* 92(1):102403. <https://doi.org/10.1016/j.flowmeasinst.2023.102403>
- Simsek O, Gumus V, Ozluk A (2023) Prediction of discharge coefficient of the trapezoidal broad-crested weir flow using soft computing techniques. *Neural Comput Appl* 35(24):17485–17499. <https://doi.org/10.1007/s00521-023-08615-9>
- Subramanya K, Awasthy SC (1972) Spatially varied flow over side weirs. *J Hydraul Div* 98:1–10
- Suykens JAK, Vandewalle J (1999) Least-squares support-vector machine classifiers. *Neural Process Lett* 9:293–300. <https://doi.org/10.1007/s11277-022-09500-9>
- Swamee PK, Pathak SK, Ali MS (1993) Analysis of rectangular side sluice gate. *J Irrig Drain Eng* 119:1026–1035. [https://doi.org/10.1061/\(asce\)0733-9437\(1993\)119:6\(1026\)](https://doi.org/10.1061/(asce)0733-9437(1993)119:6(1026))
- Tao H, Jamei M, Ahmadianfar I, Khedher KM, Farooque AA, Yaseen ZM (2022) Discharge coefficient prediction of canal radial gate using neurocomputing models: an investigation of free and submerged flow scenarios. *Eng Appl Comput Fluid Mech* 16(1):1–19. <https://doi.org/10.1080/19942060.2021.2002721>
- Yamini OA, Mousavi SH, Kavianpour MR, Ghaleh RS (2021) Hydrodynamic performance and cavitation analysis in bottom outlets of dam using CFD modelling. *Adv Civ Eng*. <https://doi.org/10.1155/2021/5529792>
- Zaji AH, Bonakdari H, Khodashenas SR, Shamshirband S (2016) Firefly optimization algorithm effect on support vector regression prediction improvement of a modified labyrinth side weir's discharge coefficient. *Appl Math Comput* 274:14–19. <https://doi.org/10.1016/j.amc.2015.10.070>
- Askeroğlu MH (2006) Combined flow over trapezoidal and below gates. M.Sc. Thesis, Institute of Science and Technology, Gazi University
- Domínguez S, Francisco J (1959) *Hidráulica*
- Kartal V (2022) Experimental and numerical analysis of combined weir-gate flow in lateral flows. Ph.D. Thesis, Institute of Applied Science, Firat University
- Negm AM (2002) Modeling of submerged simultaneous flow through combined weirs and gates devices. In: *Advances in Hydro-Science and -Engineering, Proceedings of 5th International Conference on Hydro-Science and -Engineering*. Warsaw
- Springer Nature or its licensor (e.g. a society or other partner) holds exclusive rights to this article under a publishing agreement with the author(s) or other rightsholder(s); author self-archiving of the accepted manuscript version of this article is solely governed by the terms of such publishing agreement and applicable law.

